Standard Load Method: A New Calibration Technique for Material Characterization at Terahertz Frequencies

Alireza Kazemipour, Johannes Hoffmann, Michael Wollensack, Martin Hudlička, *Senior Member, IEEE,* Jürg Rüfenacht, Daniel Stalder, Djamel Allal, Gregory Gäumann, and Markus Zeier

***Abstract*— Measuring the material parameters with a vector network analyzer (VNA) usually requires time-domain gating and complicated free-space calibrations. At terahertz frequencies, classic calibrations become more problematic and uncertainty calculation for time gating is not clearly defined. The here investigated method skips these steps and is based on normalization to a "Thru" connection and analyzing error terms and multiple-reflection phenomena (ripples). It is shown that at specific frequencies, the ripples are very small. Based on this, the "standard load" method is introduced, which simplifies the error correction for transmission and reflection measurements for the whole frequency range. Results are presented in 75–110- and 500–750-GHz bands with a quasi-TEM free-space setup. Various material slabs (thin, thick, lossy, and low-loss) have been tested to show the reliability and general usefulness of the method. This method that is initially based on a "Thru" connection only provides a simple and low-cost alternative to the conventional standards (Line, Match, Short, and so on) and calibration techniques.**

***Index Terms*— Material characterization, measurement uncertainty, parameter extraction, standard load, vector network analyzer (VNA) time gating.**

I. Introduction

MEASUREMENT of material parameters (complex permittivity and permeability) at higher frequencies is still not a completely solved topic with important applications in telecommunications, autonomous vehicles, biomedical, space technology, and more. The spectroscopy done by using vector network analyzers (VNAs) has been recently extended to millimeter-wave/terahertz (THz) domain with the availability of millimeter-wave frequency extenders. The VNAs can operate up to 110 GHz and commercial frequency extension units are used for higher bands, currently up to 1.1 THz [1]. Free-space techniques are useful for measurement of intrinsic properties of samples, which cannot be inserted into waveguide because of dimensional restrictions. Quasi-optical devices are used in this case to convert waveguide modes into free-space propagation. A Gaussian beam assumption is often used to design and optimize the quasi-optical systems, especially in the THz domain [2]. The setup typically consists of receiving and transmitting antennas, mirrors, dielectric lenses to focus the beam, and the VNA as the core measuring unit [3], [4]. Calibration of the system both at the waveguide flanges [1], [5] and antenna apertures [6] is problematic due to precision-positioning challenges and lack of suitable standards. Recently, a compact mode converter (SWISSto12@ MCK [7]) has become commercially available, which uses a set of two long corrugated antennas with a suitable aperture feature to clamp a material slab [8]. The manufacturer suggests a classic calibration method and time-domain gating (as often used in many other commercial and research-oriented setups) of the measured scattering parameters (S-parameters) [9]. This calibration technique was used, e.g., for measurement of S-parameters and consequent retrieval of material parameters in [10] and [11]. Other calibration techniques, such as the through-reflection-line (TRL), were tested using this system as well [12]. Successful time-domain gating of the measured S-parameters [13] can help to extract the material permittivity with various techniques. However, the reliability will depend on the uncertainties associated with the gating and filtering.

In the CPEM-20 conference abstract [14], a simple technique was introduced briefly, which can be not only useful for the material characterization setups but also for VNA calibration in general. This is of high interest because of the lack of reliable Match, offset-Short, and Line standards at terahertz frequencies, where the very small wavelengths make challenging the precise positioning and repeatability of measurements. Actually, nonperfect calibration together with (the often-used) time-domain gating attributes more uncertainties to the final extracted material parameters.

In this article, we try to present alternative solutions to make the calibration process more accessible (in terms of complexity, cost, feasibility, and reliability) and establish simple comprehensive error-correction methods.

Manuscript received February 15, 2021; accepted April 24, 2021. Date of publication May 5, 2021; date of current version May 18, 2021. This work was supported in part by the 18SIB09 TEMMT (Traceability for Electrical Measurement at Millimeter-Wave and Terahertz Frequencies for Communications and Electronics Technologies) Project. TEMMT has received funding from the European Metrology Programme for Innovation and Research (EMPIR) Programme co-financed by the Participating States and from the European Union's Horizon 2020 Research and Innovation Programme. The Associate Editor coordinating the review process was Dr. Ron Goldfarb.
(Corresponding author: Alireza Kazemipour.)

Alireza Kazemipour, Johannes Hoffmann, Michael Wollensack, Jürg Rüfenacht, Daniel Stalder, Gregory Gäumann, and Markus Zeier are with the Swiss Federal Institute of Metrology (METAS), CH-3003 Bern, Switzerland (e-mail: alireza.kazemipour@metas.ch).

Martin Hudlička is with the Czech Metrology Institute, 102 00 Prague, Czech Republic.

Djamel Allal is with the Laboratoire National de Métrologie et d'Essais (LNE), 75015 Paris, France.
Digital Object Identifier 10.1109/TIM.2021.3077660

This work is licensed under a Creative Commons Attribution 4.0 License. For more information, see https://creativecommons.org/licenses/by/4.0/

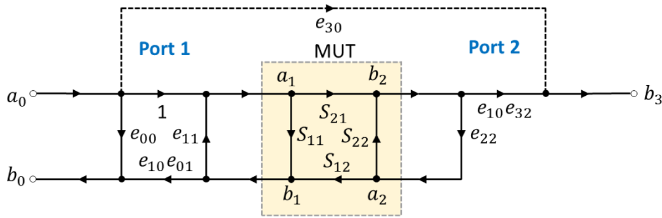

Fig. 1. VNA measured S-parameters ($S_{ij.\mathrm{M}}$), error terms (e_{ij}), and DUT S-parameters (S_{ij}). The error terms are: e_{00} = directivity, e_{11} = source match, ($e_{10}e_{01}$) = reflection tracking, ($e_{10}e_{32}$) = transmission tracking, e_{22} = load match, and e_{30} = leakage.

The theory part and results are organized and presented as follows. Section II is dedicated to transmission measurement based on one standard only: "Thru." The feasibility of full error correction is studied further with the analysis of the most sensitive parameters and demonstrating the utility of the "best points." Several examples with various materials (low-loss, lossy, thin, and thick) are presented. In Section III, we introduce and discuss the concept of "Standard Load," which is established using the "best points" of Section II. Finally, in Section IV, the reflection of several material slabs is measured and analyzed based on the extended application of "Standard Load" in a one-port VNA configuration.

II. Transmission Method and Error Analysis

The measurement is initiated with a simple normalization process. The transmission of material-under-test (MUT) loaded setup divided by the transmission of a direct Thru. It is followed by analyzing the error terms in order to correct and reduce the standing-wave effects. Fig. 1 shows the VNA measurement error terms and the relations between $S_{(\mathrm{measured})}$ and S_{MUT}.

The following relations can be derived from Fig. 1:

$$S_{21M} = \frac{b_3}{a_0} = e_{30} + (e_{10}e_{32})\frac{S_{21}}{1 - e_{11}S_{11} - e_{22}S_{22} + e_{11}e_{22}\Delta_S} \quad (1)$$

where $\Delta_S = S_{11}S_{22} - S_{21}S_{12}$.

Ignoring the leakage term (e_{30}) in Fig. 1 and assuming for MUT ($S_{21.\mathrm{MUT}}$, $S_{11} = S_{22}$) and Thru connection ($S_{21} = S_{12} = 1$ and $S_{11} = S_{22} = 0$) yield

$$\frac{S_{21.M}(\mathrm{MUT})}{S_{21.M}(\mathrm{Thru})} = S_{21}(\mathrm{MUT}) \times \frac{1 - e_{11}e_{22}}{1 + e_{11}e_{22}\left(S_{11}^2 - S_{21}S_{12}\right) - S_{11}(e_{11}+e_{22})}. \quad (2)$$

We can analyze (2) by looking at the Fabry–Pérot effects inside a material slab (MUT). In fact, S_{21}, S_{12}, S_{11}, and S_{22} are intrinsic parameters of the MUT that we try to measure. Nevertheless, it is known that if the material is not very lossy, $|S_{21}|$max. and $|S_{11}|$min. occur simultaneously at the frequency points [15], [16], for which $\varphi(S_{21}) = n\pi$. Therefore, at $|S_{11}|$min. ($|S_{21}|$max. $\approx$ 1 & $|S_{11}|$min. $\approx$ 0, for thin low-loss materials)

$$\frac{S_{21.M}(\mathrm{MUT})}{S_{21.M}(\mathrm{Thru})} = S_{21}(\mathrm{MUT})\frac{1 - e_{11}e_{22}}{1 - e_{11}e_{22}(S_{21}S_{12})}. \quad (3)$$

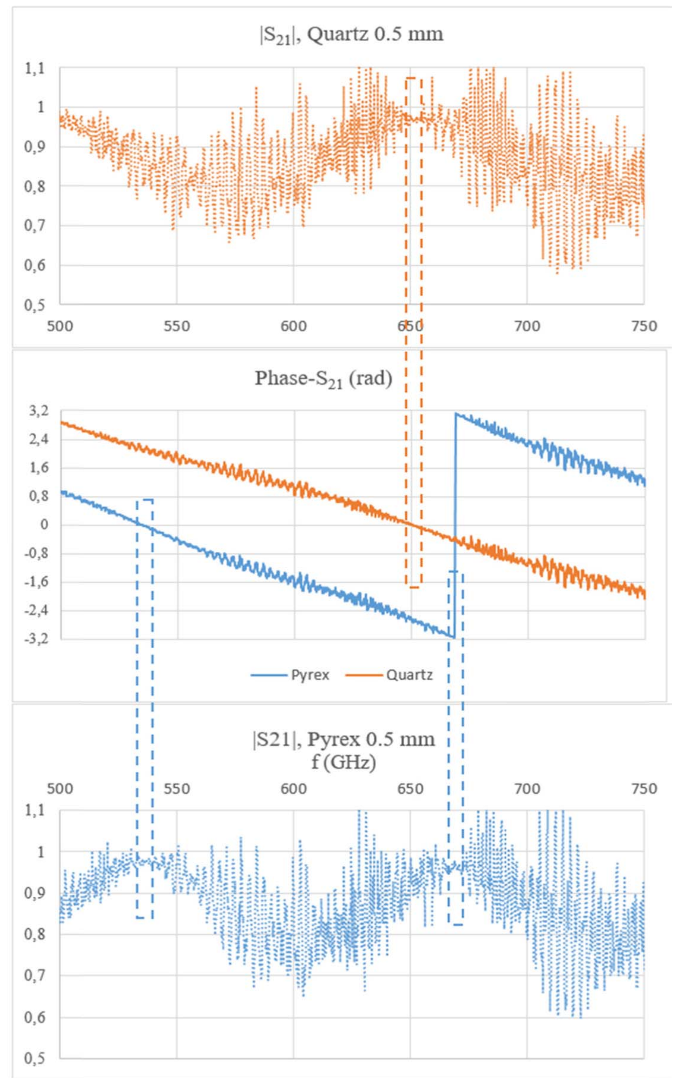

Fig. 2. S_{21} raw, phase (rad), and amplitude: Pyrex and Quartz 500-750 GHz. The best points (fewer ripples) are at $|S_{21}|_{\mathrm{Max.}}$ and $\varphi(S_{21}) = n\pi$.

As deduced from (2), error terms and system multiple reflections on S_{21}(MUT) all approximately vanish for maximum $|S_{21}|$ and $\varphi(S_{21}) = n\pi$ points (visible on both $|S_{21}|$ and $\varphi(S_{21})$ "measured" plots). This is demonstrated for two thin low-loss materials [see Fig. 2: Pyrex and Quartz, 500–750 GHz, S_{21}.raw = $S_{21.\mathrm{M}}(\mathrm{MUT})/S_{21.\mathrm{M}}(\mathrm{Thru})$].

A very first application of this simple fact can be to check the validity and reliability of any time gating, filtering/averaging, or free-space calibration in general, at these specific frequency points. As shown, these points give reliable results without calibration or any data processing. Besides, the associated uncertainties are expected to be smaller because the normalization process usually reduces effectively the correlated uncertainty terms (cable effects, nonperfect standards, and so on).

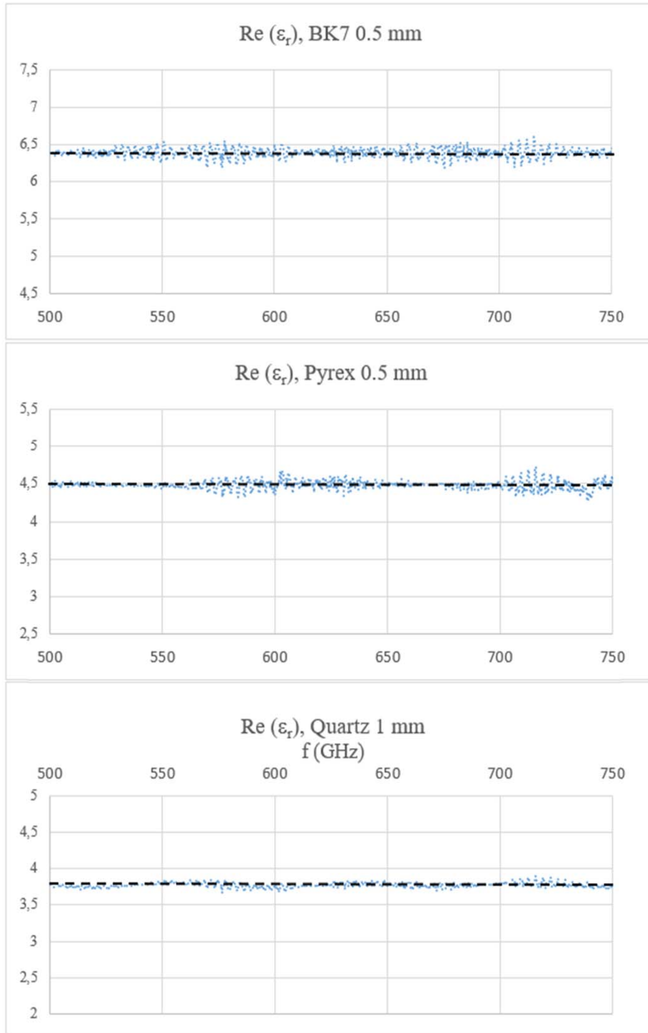

Fig. 3. Re (ε_r): permittivity of thin glass-type samples, raw data (...blue), and fitted line based on "best points = less ripples."

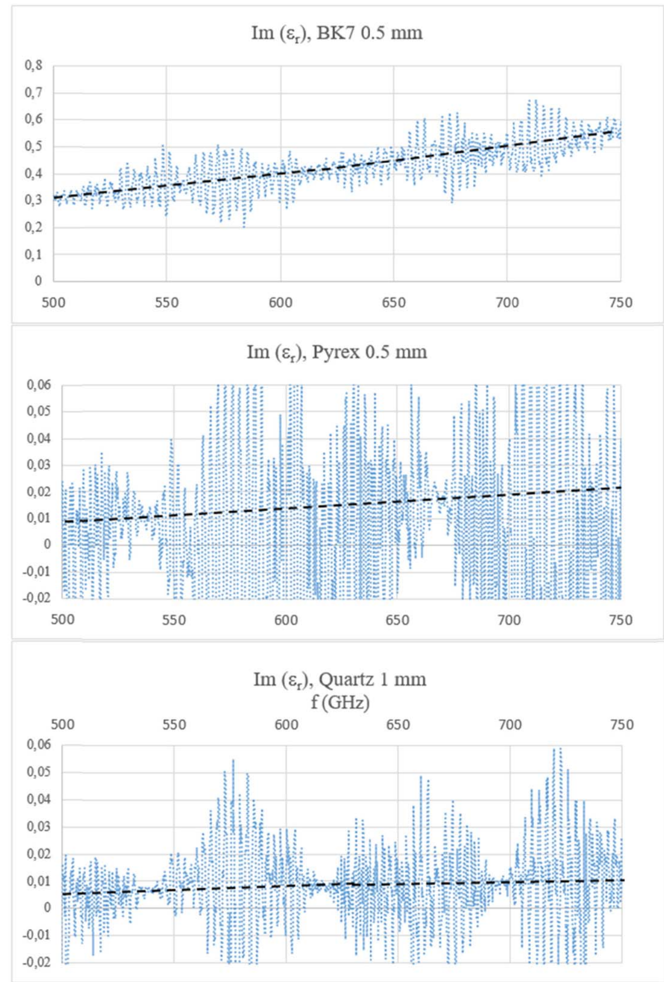

Fig. 4. Im (ε_r): permittivity of thin "glass" samples, raw data (...blue), and fitted line based on "best points."

Actually, reliable results of S_{21} even for a limited number of points in a given frequency range are of interest. Some commonly used homogeneous materials have nearly constant permittivity (slight rising of imaginary part with the frequency) in the millimeter-wave/terahertz domain. Figs. 3 and 4 show the extracted permittivity of some thin materials affected by multiple reflections from the initial measured S-parameters.

Permittivity can be evaluated at the "best" points of S_{21} (fewer ripples on the phase and amplitude) using relevant extraction methods [15]. This fact can be checked and validated for thicker materials where $|S_{21}|_{\max}$ is repeated a few times along the exploited frequency range. This can be a simple helpful hint for the initial values of real and imaginary parts of permittivity to be used further in extraction techniques, if needed. Furthermore, these points are enough to characterize a thin HRSi slab in the entire frequency range (see Section III).

This is advantageous because these points not only have the least errors associated with the measured transmission parameter but also give the best uncertainty associated with the extraction process [15]. Therefore, reliable results are achieved in terms of measured S_{21} and the relevant extracted permittivity.

The imaginary part of permittivity is usually rising with the frequency, and here, we can consider the "best points" (which have the least ripples) again. The fitted line between these zones can be a good estimation of Im (ε_r) for the whole frequency range (see Fig. 4) to give the quantitative results from Fig. 4: $0.3 < \text{Im}(\varepsilon_r) < 0.6$ for BK7, $0.01 < \text{Im}(\varepsilon_r) < 0.02$ for Pyrex, and $0.005 < \text{Im}(\varepsilon_r) < 0.012$ for Quartz, in the 500–750-GHz band.

It is observed that higher thicknesses and increased internal losses can reduce the detected multiple reflections.

More results are presented for thicker or lossy materials (see Fig. 5) for which multiple-reflection effects are less apparent because of energy damping in the MUT. Actually, polyoxymethylene (POM) is a relatively low-loss material (Im (ε_r) $\sim$ 0.06), but the fact of using a thicker slab (4 mm) increases the overall losses of the MUT in 500–750-GHz band and therefore reduces the multiple-reflection effects. Measurement results are based on free-space techniques by using uncalibrated VNA and the associated frequency extensions.

The estimated uncertainty for Re (ε_r) is 3%–4% and 10%–15% for Im (ε_r). It depends on the material thickness uncertainty $\delta d/d$ [the most important contribution to $\delta\text{Re}(\varepsilon_r)$], $|S_{21}|$, extraction process, and other parameters [15].

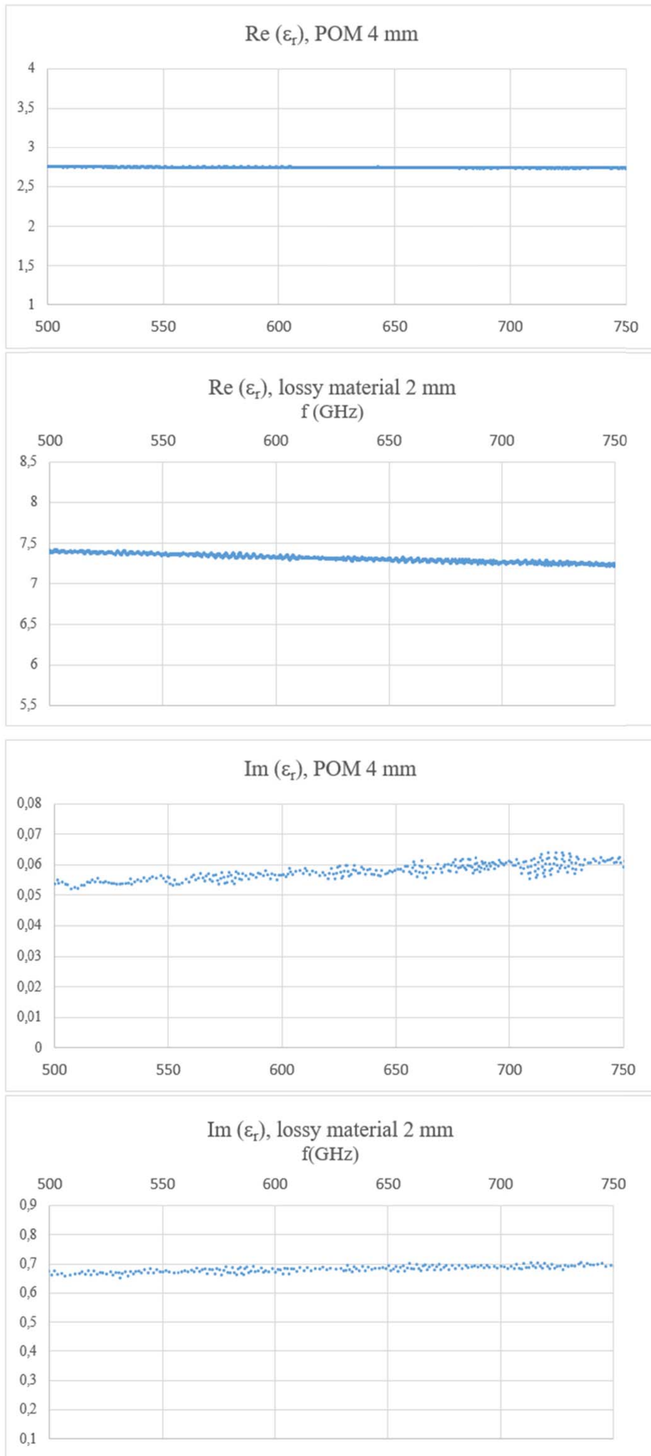

Fig. 5. Permittivity of thicker samples. Top: Re(ε_r). Bottom: Im(ε_r), raw data.

The quasi-optical device (waveguide to free-space transition) here is a commercially available mode convertor [MCK Swissto12@ [7], a set of two corrugated horn antennas (see Fig. 6)]. A well-designed long-tapered corrugated horn antenna can convert waveguide propagation modes into TEM free-space mode on its aperture where the MUT is installed. The system should be characterized to reduce possible systematic errors related to propagation modes, matching, losses, and aperture/gap scattering.

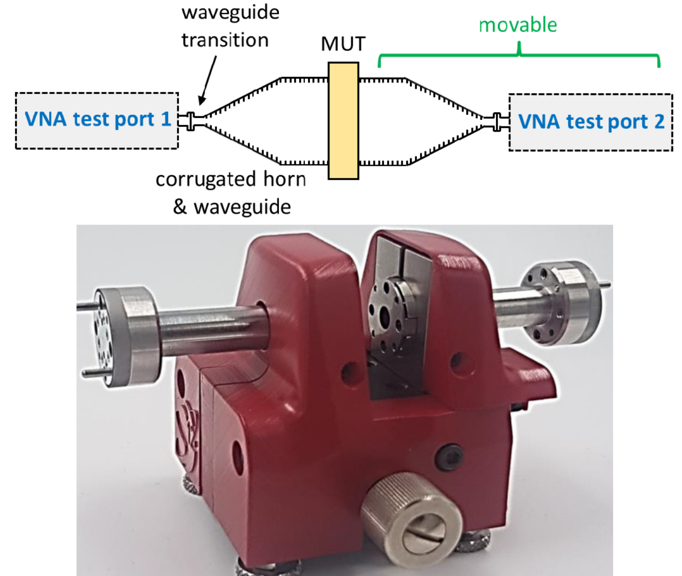

Fig. 6. Measurement setup—MCK connected to the VNA frequency extension modules with the MUT clamped between the two antennas apertures.

In this section, the results were presented based on raw transmission parameters where the effects of multiple reflection are propagated to the final extracted permittivity. We also showed the role of the MUT itself to reduce these effects (thicker slabs and/or lossy materials)

In the following, a new technique is presented, called "standard load" method, to correct and reduce the ripples without filtering/averaging or time gating.

III. "Standard Load" Method

Fabry–Pérot relations (4) describe the S-parameters of MUTs as a function of T and Γ

$$S_{11} = \frac{\Gamma(1-T^2)}{1-\Gamma^2 T^2}, S_{21} = \frac{T(1-\Gamma^2)}{1-\Gamma^2 T^2}. \tag{4}$$

The "standard load" method is based on the reconstruction of S-parameters with characterized T and Γ. This is possible under special conditions for some material slabs with the simple method in Section II. The phase of T (proportional to $f.d.\sqrt{\varepsilon_r'}$) can be calculated from the measured $\phi(S_{21})$ [15] with a high accuracy especially at "best points." Given d (the material thickness), $\sqrt{\varepsilon_r'}$ and consequently Γ (real-number for low-loss materials, $|\Gamma| = \sqrt{\varepsilon_r'} - 1/\sqrt{\varepsilon_r'} + 1$) are determined. $|T|$ is the most critical and can be determined (from quadratic (4) once Γ is known) with high accuracy only for some specific material slabs. An example of such a suitable candidate is a thin HRSi (highly-resistive silicon) sample (see Fig. 7).

The measured $|S_{21}|$max. of HRSi is equal to 1 (very close to 1 with negligible errors and less ripples) with three repeated maximums.

Given Γ^2 positive, real, and smaller than 1, from (4), $|S_{21}|$max. $\leq |T| \leq 1$ and we can conclude $|T| = 1$ for the whole frequency range.

Therefore, with characterized/known T and Γ for HRSi-0.4 mm, its rebuilt S_{11} and S_{21} can be calculated from (4) (see Fig. 8).

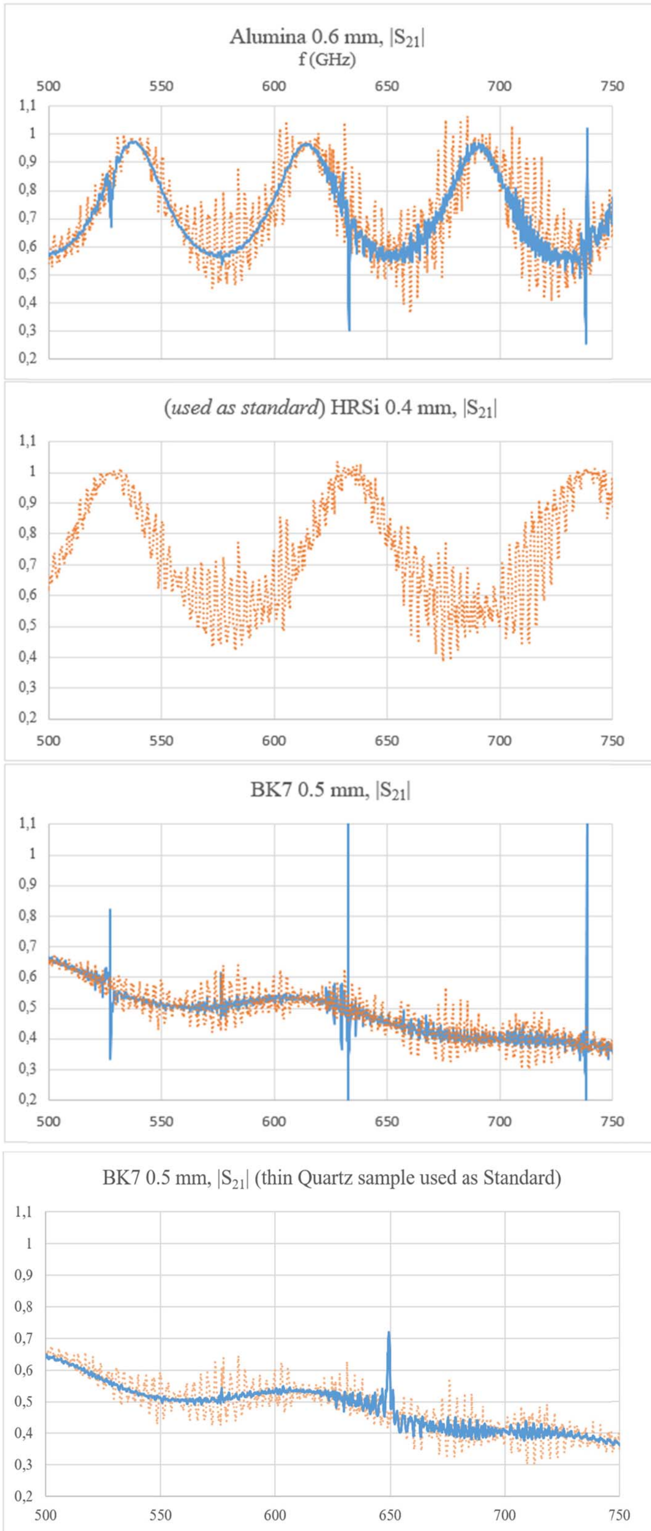

Fig. 7. $|S_{21}|$-raw (...) and $|S_{21}|$-corrected (—) with a thin silicon slab as "standard load." Bottom: $|S_{21}|$ of the BK7 sample corrected with another standard (quartz 0.5 mm of Fig. 2) to show the feasibility of "singularity" points removal.

From the VNA model [see Fig. 1 and (1) and (2)], we can see that the term "S_{11}(MUT) $(e_{11}+e_{22})$" has the most important contributions to the ripples of $|S_{21}|$. The characterized "Standard load" helps to calculate "$e_{11}+e_{22}$" (ignoring $e_{11}.e_{22}$) from (2) by comparing the raw measurement results of this load (here, HRSi 0.4 mm) to the rebuilt one.

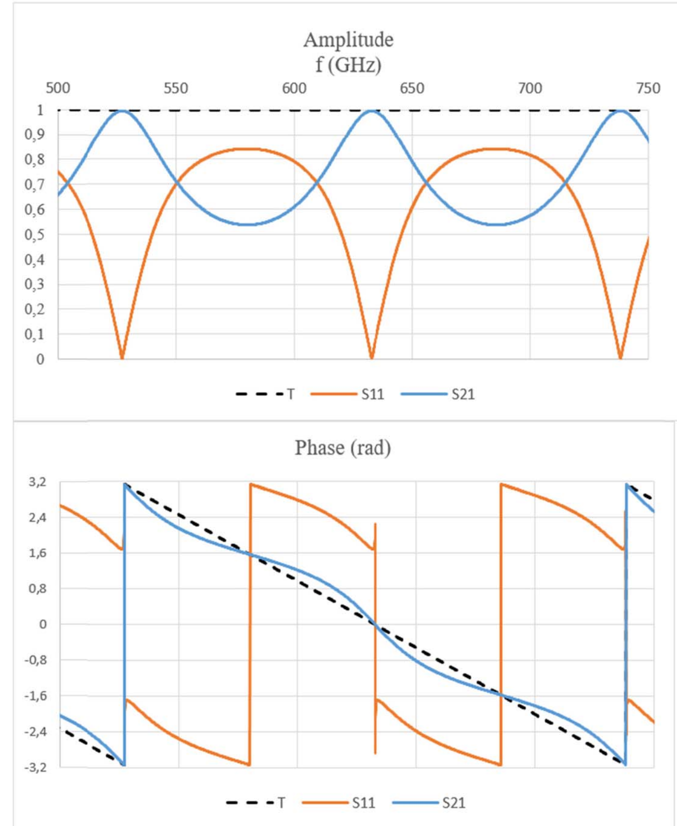

Fig. 8. Rebuilt S-parameters of HRSi-0.4 mm from (4).

The terms e_{11} and e_{22} are complex quantities with both $|e_{11}|$ and $|e_{22}| < 1$ (less than 0.25, for our system) and $|e_{11} \cdot e_{22}| \ll 1$.

From (2), we can, therefore, calculate

$$(e_{11}+e_{22})S_{11.\text{Rebuilt}} = 1 - \frac{S_{21.\text{Rebuilt}}}{S_{21.\text{Raw}}}. \quad (5)$$

Singularity points appear where $|S_{11}|$ (standard) ≈ 0.

The abovementioned method has been successfully tested for various MUTs in the 500–750- and 75–110-GHz bands and the results are presented in Figs. 7 and 9.

It is interesting to see the role of singularity points related to the standard load. These points can be removed by using different thicknesses of the same standard material or different material slabs, which can be characterized as standard (Fig. 7, bottom).

The surface flatness of the standards and MUTs and the contact quality are very important parameters to have more reliable error correction. The peaks observed in Fig. 7 are due to singularity issues of the standard slab at certain frequencies.

Classic techniques exist (mostly in EMC applications) to reduce S_{11}(MUT) (from the VNA point-of-view): 1) tilting the MUT slab and 2) improving the source-match parameter by inserting low-reflection absorbers to decrease "e_{11} and e_{22}" simultaneously. These techniques can be used in material measurements (transmission configuration); however, special care

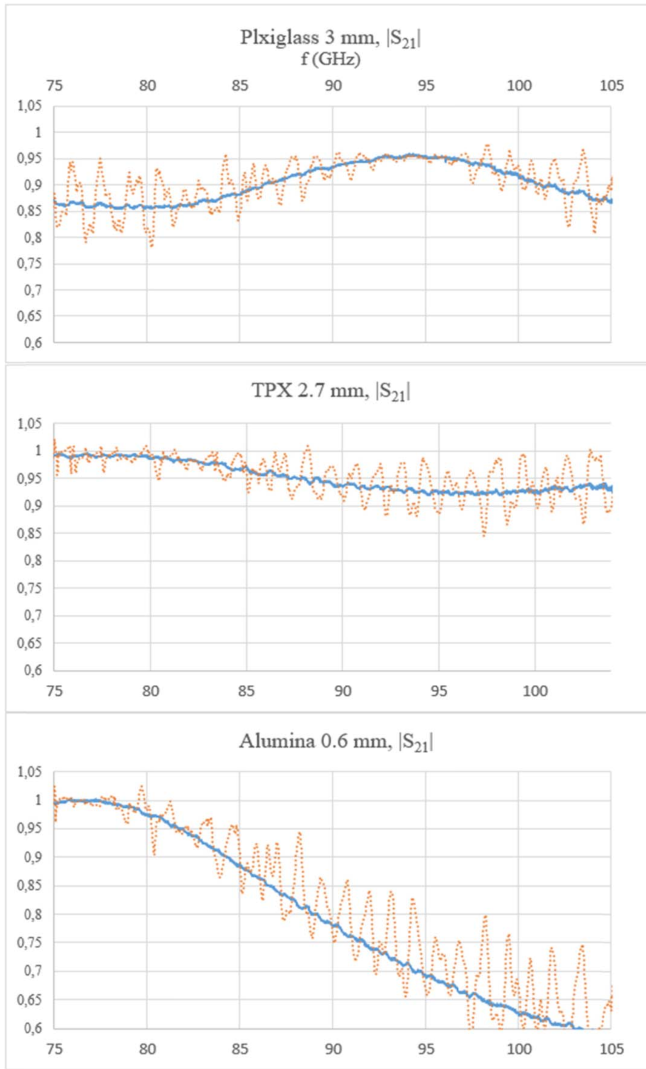

Fig. 9. $|S_{21}|$-raw (...) and $|S_{21}|$-corrected (—) of different material slabs.

is needed regarding the repeatability/positioning and scattering and for determining the effective thickness.

IV. Reflection Measurement

In Sections II and III, we showed that the complex permittivity can be extracted from the measured transmission parameter. However, the reflection measurement can be needed for special applications and particularly for extracting the permeability of magnetic materials.

Similar to S_{21} in Section III, the rebuilt S_{11} from (4) of the standard load can open the way to correct the reflection parameter as well. Fig. 10 and (6) show one-port VNA measurement error terms and the relations between $S_{11(\text{measured})}$ and $S_{11(\text{MUT})}$

$$S_{11}, M(\text{MUT}) = e_{00} + \frac{e_{10}e_{01}}{1 - e_{11}S_{11}(\text{MUT})} S_{11}(\text{MUT}). \quad (6)$$

Let us start with a simple elementary calculation of errors: e_{00} from the absorber, determining $e_{10}e_{01}$ from a known load (Short or standard load) and leaving e_{11} uncalculated, for instance.

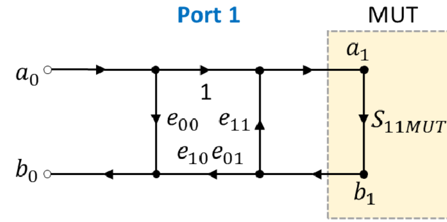

Fig. 10. VNA 1-port model and error terms (e_{ij}) for reflection measurement.

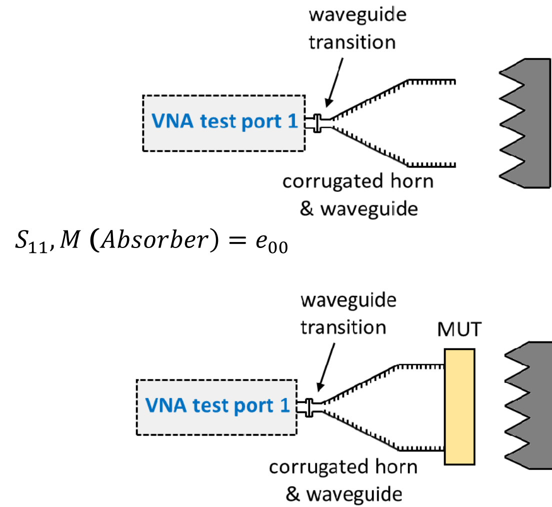

consecutive measurements for MUT and standard-load with uncalibrated VNA

Fig. 11. Reflection measurement configuration.

Three consecutive measurements with noncalibrated VNA, absorber, standard.load, and MUT, (see Fig. 11) lead to

$$\begin{aligned} S_{11}, M(\text{Absorber}) &= e_{00} \\ S_{11}, M(\text{Stand.}) - e_{00} &= \frac{e_{10}e_{01}}{1 - e_{11}S_{11}(\text{Standard})} S_{11}(\text{Stand.}) \\ S_{11}, M(\text{MUT}) - e_{00} &= \frac{e_{10}e_{01}}{1 - e_{11}S_{11}(\text{MUT})} S_{11}(\text{MUT}) \\ S_{11}(\text{MUT}) &= S_{11}(\text{Standard}) \frac{S_{11}, M(\text{MUT}) - e_{00}}{S_{11}, M(\text{Standard}) - e_{00}} \\ &\quad \times \frac{1 - e_{11}S_{11}(\text{MUT})}{1 - e_{11}S_{11}(\text{Standard})}. \end{aligned} \quad (7)$$

The results are shown in Fig. 12 with small ripples associated with e_{11} as expected. This is to show the reliability of the method even with only one standard load comparing to a conventional Short (metal plate).

Here, also, a thin HRSi slab (0.4 mm, $\varepsilon_r = 11.7 - j0$, with 5% estimated uncertainty) slab can be used as standard load (Fig. 12, bottom). The peaks on the curves are due to singular points of the standard slab where $|S_{11}| \approx 0$ (this is also visible on the transmission measurements, Fig. 7).

A more optimal choice could be a thick low-loss, low-refractive slab (POM, for example: 15 mm, $\varepsilon_r = 2.75 - j0.06$, with 3% estimated uncertainty), which was successfully characterized with a Thru, only. From Fig. 5, it can be expected that for a thick slab (higher loss), the multiple-refection effects

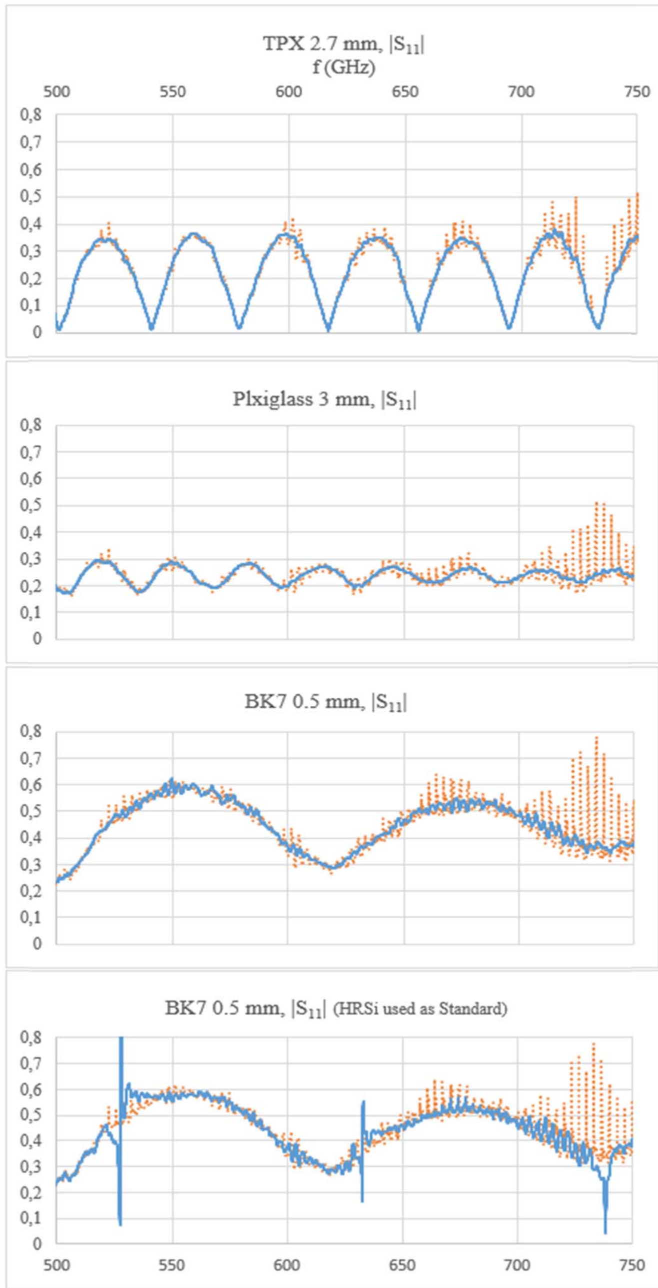

Fig. 12. Measured $|S_{11}|$ for different materials, standard-load, POM (—) comparing to metallic-plate Short (…). Bottom: with standard-load, HRSi (—).

disappear, therefore resulting in a more accurate permittivity for all the frequencies.

The singularity peaks, therefore, vanish with more losses in a thick standard ($|S_{21}|$ is not very close to one and $|S_{11}|$ is not close to zero). The quality of material-to-antenna-aperture contact is important to minimize the air gaps. These imperfections can be observed more apparently at the higher frequencies both for reflection and transmission parameters.

From (7), the uncertainty sensitivity coefficients can be determined by calculating partial derivatives of S_{11}(absorber) and S_{11}(Standard). As a result, we can see that the uncertainty is directly proportional to δS_{11}(Standard). Moreover, the effect of the imperfect absorber is more visible when S_{11}(MUT) and S_{11}(Standard) differ largely.

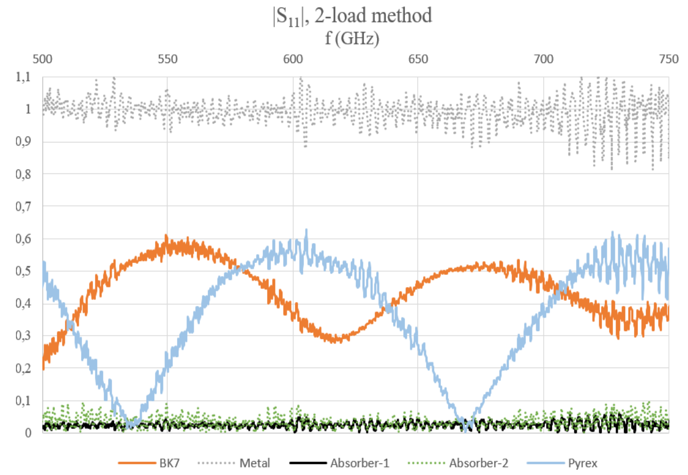

Fig. 13. Measured $|S_{11}|$ of different materials by the two-load method: metal plate, BK7 0.5 mm, Pyrex 0.5 mm, and two different absorbing materials.

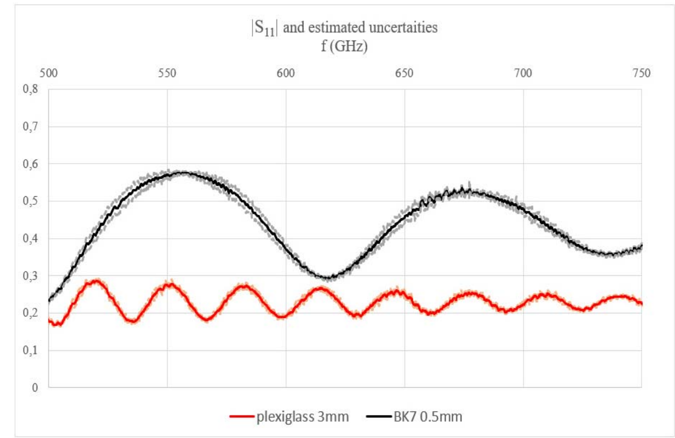

Fig. 14. Measured $|S_{11}|$ and uncertainties of BK7 0.5 mm and Plexiglass 3 mm.

The method is extended to two-load (without using an absorber) to check its overall reliability and, in addition, the repeatability of measurements. Applying (6) for two standard loads and MUT leads to

$$\begin{aligned} S_{11}(\mathrm{MUT}) &= \frac{S_{11}(Std.2)[S_{11},M(Std.1) - S_{11},M(\mathrm{MUT})]}{S_{11},M(Std.1) - S_{11},M(Std.2)} \\ &\quad - \frac{S_{11}(Std.1)[S_{11},M(Std.2) - S_{11},M(\mathrm{MUT})]}{S_{11},M(Std.1) - S_{11},M(Std.2)} \end{aligned} \tag{8}$$

where *Std.1* and *Std.2* are the characterized/known standards (the equation is simplified by ignoring the effects of e_{11}).

In this case, the quality of absorbers and metallic plates can be tested as well (see Fig. 13). Two standard loads used here are: POM and BK7 (4 mm, $\varepsilon_r = 6.45 - j0.45$, with 3% estimated uncertainty).

The error term e_{11} is not yet corrected and its effects are usually more visible for the higher values of $|S_{11}|$.

The three-load method [17] can help to correct all the error terms if three suitable standards are available and the relevant measurements can be performed with minimum

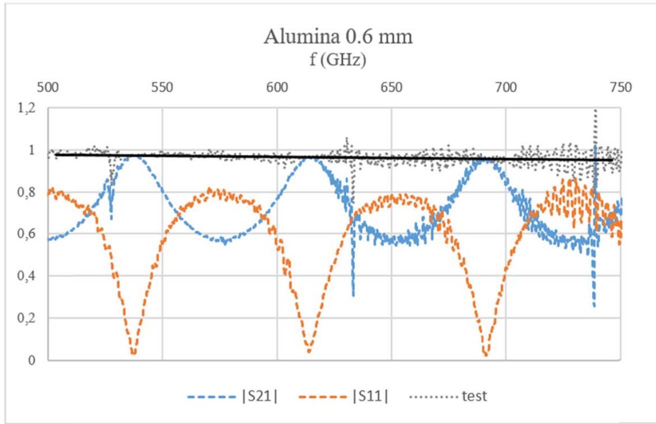

Fig. 15. Test of validity for measured $|S_{21}|$ and $|S_{11}|$ (...test $= \sqrt{|S_{11}|^2 + |S_{21}|^2}$).

systematic errors (air gap, material surface quality, contact and positioning, and so on). We used this method (three standards: absorber, POM, and BK7) to calculate the port-match parameter $|e_{11}|$, including the antenna. Its value is estimated around 0.2 ($\approx$−14 dB) for most of the frequencies but can rise up to 0.3 ($\approx$−10 dB) for the higher edge: 700–750 GHz. This could explain the more visible ripples at these frequencies for all the transmission and reflection measurements.

Using the analytical relations of two- and three-load methods, we can calculate the uncertainty propagation from the standards to the measured S_{11}(MUT). An example is presented here (Fig. 14) to show $|S_{11}|$ with the estimated uncertainties. The uncertainties of approximately 3% of Standard-loads' permittivity can impose the standard deviation of 0.003–0.02 on a BK7 thin slab and 0.003–0.01 on a thicker Plexiglass slab.

The phase of S_{11} is more sensitive to the surface quality and MUTs positioning. A parallel way is to utilize (4) to directly rebuild the phase of S_{11} based on the given phases of S_{21} and T from transmission measurements and the "best points" advantage.

We present an additional validity check for measured S-parameters after error correction, averaging/filtering, and time gating. Let us look at the energy relation between the S-parameters: $|S_{11}|^2 + |S_{21}|^2$ = constant ($\approx$1, for very low losses) $= |S_{21}|^2$max (proved at the "best points" where the ripples are at lowest: $|S_{21}|^2$max, $|S_{11}|^2$min ≈ 0).

This can be extended to all the frequencies (very low-loss slab):

$$|S_{11}|^2 + |S_{21}|^2 = |S_{21}|^2\text{max}. \tag{9}$$

This basic simple relation is a reliable test to check the validity and diagnose the probable systematic errors, which may arise due to time gating, averaging, imperfect error correction, and the setup robustness in general.

Fig. 15 shows the validity test of $|S_{11}|$ and $|S_{21}|$ measurements of a low-loss MUT (Alumina 0.6 mm slab). The raw data have been corrected partially by the two-load method and then checked by the energy relation (9). Apart from singularity points due to HRSi standard load, small deviations are observed around 520 GHz probably related to imprecise reflection measurement.

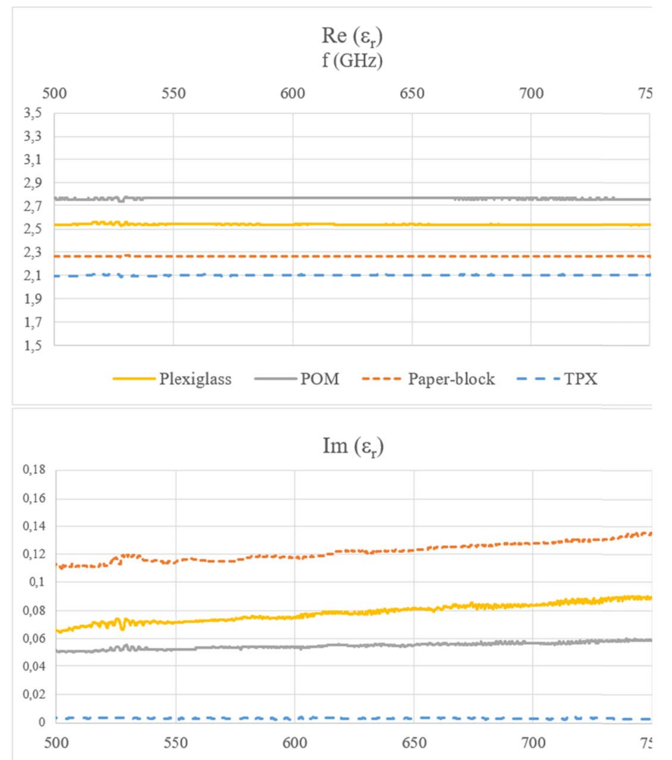

Fig. 16. Permittivity of some low-loss materials.

In Fig. 16, we present the extracted permittivity (real and imaginary parts) of some low-loss materials for which S-parameters have been measured and corrected by the standard-load method: "Transmission" in Section III and "Reflection" in Section IV.

The transmission/reflection extraction technique [16] is used to calculate Re (ε_r) and Im (ε_r) of Plexiglass (3 mm) and paper block (8 mm). For the very low-loss materials, TPX (2.7 mm) and POM (6.5 mm), the simplified Tr-only method [15] is applied. Extraction of Im (ε_r) of very low-loss materials, such as TPX and PTFE, is quite challenging in the millimeter-wave/terahertz domain. The results and uncertainties presented in this article can be compared with some published data in [6] and [10]–[12]. Actually, there are not many published results regarding VNA-based setups for frequencies beyond 500 GHz, and the results may be compared with optical methods, which cover frequencies from submillimeter domain to a few THz [18], [19].

V. Conclusion

Simple techniques are presented to measure material parameters in free space (using quasi-TEM mode convertors) without classic calibration and time-domain gating. Based on a "Thru" connection only, "standard load" method is introduced and developed for transmission and reflection measurements. Results are presented and discussed for various types of materials for two waveguide frequency ranges: 500–750 and 75–110 GHz.

This feasible and low-cost alternative could be of high interest because of lack of reliable classic Short, Match, and Line standards at THz frequencies. The method can be used for in-waveguide applications (at lower frequencies) as well, and therefore, it is helpful for the VNA calibration, in general.

A detailed uncertainty analysis can show the most sensitive parameters and find suitable solutions to improve the accuracy. One of them can be to use different thicknesses of the same material as standard (cut/machined from a unique batch) to reduce the uncertainties associated with Γ.

This technique can be used to easily measure and characterize thick ceramics samples and two-layer materials as well.

ACKNOWLEDGMENT

The authors would like to thank Prof. Axel Murk (University of Bern, Bern, Switzerland), Dr. Xiaobang Shang (NPL, U.K.), Dr. Alexandre Dimitriades (SWISSto12, Switzerland), and Dr. Fabian Emons (RPG, Germany) for their valuable cooperation.

REFERENCES

[1] D. K. George, A. Charkhesht, and N. Q. Vinh, "New terahertz dielectric spectroscopy for the study of aqueous solutions," *Rev. Sci. Instrum.*, vol. 86, no. 12, Dec. 2015, Art. no. 123105.

[2] P. F. Goldsmith, *Quasioptical Systems: Gaussian Beam Quasioptical Propagation and Applications*. Piscataway, NJ, USA: Wiley, 1998.

[3] A. Kazemipour *et al.*, "Design and calibration of a compact quasi-optical system for material characterization in millimeter/submillimeter wave domain," *IEEE Trans. Instrum. Meas.*, vol. 64, no. 6, pp. 1438–1445, Jun. 2015.

[4] T. Tosaka, K. Fujii, K. Fukunaga, and A. Kasamatsu, "Development of complex relative permittivity measurement system based on free-space in 220–330-GHz range," *IEEE Trans. THz Sci. Technol.*, vol. 5, no. 1, pp. 102–109, Jan. 2015.

[5] D. F. Williams, "500 GHz–750 GHz rectangular-waveguide vector-network-analyzer calibrations," *IEEE Trans. THz Sci. Technol.*, vol. 1, no. 2, pp. 364–377, Nov. 2011.

[6] E. Saenz, L. Rolo, K. van't Klooster, M. Paquay, and V. V. Parshin, "Accuracy assesment of material measurements with a quasi-optical free-space test bench," in *Proc. 6th Eur. Conf. Antennas Propag. (EUCAP)*, Prague, Czech Republic, Mar. 2012, pp. 572–576.

[7] *Material Characterization Kit*. Accessed: Jun. 20, 2020. [Online]. Available: https://www.swissto12.com/

[8] F. Cahill, "Design and analysis of corrugated conical horn antennas with terahertz applications," M.S. thesis, Dept. Exp. Phys., Nat. Univ. Ireland Maynooth, Maynooth, Ireland, 2015.

[9] P. G. Bartley and S. B. Begley, "Improved free-space S-parameter calibration," in *Proc. IEEE Instrum. Meas. Technol. Conf. (IMTC)*, Ottawa, ON, Canada, May 2005, pp. 372–375.

[10] A. Khalid, D. Cumming, R. Clarke, C. Li, and N. Ridler, "Evaluation of a VNA-based material characterization kit at frequencies from 0.75 THz to 1.1 THz," in *Proc. IEEE 9th UK-Eur.-China Workshop Millimetre Waves THz Technol. (UCMMT)*, Qingdao, China, Sep. 2016, pp. 31–34.

[11] Y. Wang, X. Shang, N. M. Ridler, T. Huang, and W. Wu, "Characterization of dielectric materials at WR-15 band (50–75 GHz) using VNA-based technique," *IEEE Trans. Instrum. Meas.*, vol. 69, no. 7, pp. 4930–4939, Jul. 2020.

[12] Y. Wang *et al.*, "Material measurements using VNA-based material characterization kits subject to Thru-reflect-line calibration," *IEEE Trans. THz Sci. Technol.*, vol. 10, no. 5, pp. 466–473, Sep. 2020.

[13] S. Kim, D. Novotny, J. A. Gordon, and J. R. Guerrieri, "A free-space measurement method for the low-loss dielectric characterization without prior need for sample thickness data," *IEEE Trans. Antennas Propag.*, vol. 64, no. 9, pp. 3869–3879, Sep. 2016.

[14] A. Kazemipour *et al.*, "VNA-based material characterization in THz domain without classic calibration and time-gating," in *Proc. Conf. Precis. Electromagn. Meas. (CPEM)*, Boulder, CO, USA, Aug. 2020, pp. 1–2.

[15] A. Kazemipour *et al.*, "Analytical uncertainty evaluation of material parameter measurements at THz frequencies," *J. Infr., Millim., THz Waves*, vol. 41, no. 10, pp. 1199–1217, Oct. 2020.

[16] J. Baker-Jarvis *et al.*, "Transmission/reflection and short-circuit line methods for measuring permittivity and permeability," *NIST Tech. Note*, vol. 1355, May 1992, Art. no. 012084.

[17] F. Ziade, D. Allal, M. Z. M. Jenu, and E. Bergeault, "Nonlinear modeling of RF thermistor: Application to bolometer mount calibration," *IEEE Trans. Instrum. Meas.*, vol. 60, no. 7, pp. 2445–2448, Jul. 2011.

[18] L. Oberto *et al.*, "Measurement comparison among time-domain, FTIR and VNA-based spectrometers in the THz frequency range," Metrologia, vol. 54, no. 1, pp. 77–84, 2017.

[19] M. Naftaly and R. E. Miles, "Terahertz time-domain spectroscopy for material characterization," *Proc. IEEE*, vol. 95, no. 8, pp. 1658–1665, Aug. 2007.

Alireza Kazemipour received the B.Sc. degree in electronics and telecommunications from the Sharif University of Technology, Tehran, Iran, in 1992, the M.Sc. degree in physics from Tehran University, Tehran, in 1995, and the Ph.D. degree from Télécom Paris, Paris, France, in 2002.

He was an Associate Professor and a Senior Research Engineer in Iran, France, South Korea, Malaysia, and Germany. He is currently with the Federal Institute of Metrology, Bern, Switzerland. His current research interests include electromagnetics, electromagnetic compatibility, radio frequency metrology, terahertz technology, and antennas.

Johannes Hoffmann received the Dipl.Ing. degree in electrical engineering from the University of Stuttgart, Stuttgart, Germany, in 2005, the Ing. degree from the École Nationale Supérieure des Télécommunications (ENST), Paris, France, in 2005, in the course of a double diploma program, and the Ph.D. degree from ETH Zürich, Zürich, Switzerland, in 2009.

He is currently with the Laboratory for RF and MW, Federal Institute of Metrology METAS, Bern, Switzerland. His research interest is in general measurements that involve electromagnetics, uncertainty calculation, and numerical modeling.

Michael Wollensack received the bachelor's degree in electrical and electronic engineering from the Bern University of Applied Sciences, Bern, Switzerland, in 2003.

Since 2003, he has been with the RF and Microwave Laboratory, Swiss Federal Institute of Metrology (METAS), Bern, Switzerland. His research interests are vector network analyzer (VNA) calibration algorithms and VNA measurement uncertainty calculation.

Martin Hudlička (Senior *Member, IEEE*) received the Ing. (M.Sc. equivalent) and Ph.D. degrees in electrical engineering from the Czech Technical University in Prague, Prague, Czech Republic, in 2004 and 2007, respectively.

In 2007, he joined the Department of Primary Metrology of RF Electrical Quantities, Czech Metrology Institute, Prague, where he currently works as a Metrologist and a Researcher. His research interests include microwave and millimeter-wave measurements and modern communication technologies.

Jürg Rüfenacht received the bachelor's degree in electrical and electronic engineering from the Bern University of Applied Sciences, Bern, Switzerland, in 1986.

From 1986 to 1998, he was with the Research and Development Department, Swisscom (formerly Swiss PTT), Bern. In 1998, he joined the Federal Institute of Metrology (METAS), Bern, where he is currently with the RF and Microwave Laboratory.

Daniel Stalder was born in Thun, Switzerland, in 1981. He received the B.Sc. degree in electrical engineering from the Berne University of Applied Sciences, Bern, Switzerland, in 2006.

Since 2012 he has been a Staff Scientist at the RF and Microwave Laboratory, Federal Institute of Metrology (METAS), Bern, Switzerland. His main activities include RF and microwave metrology for power and noise.

Djamel Allal received the Ph.D. degree in electronics from the University of Lille, Lille, France, in 1997.

He joined the Laboratoire National de Métrologie et d'Essais (LNE), Paris, France, in 2001, where he has been mainly working in research activities in the field of RF and microwave metrology. His current activities include the development of measurement standards in power and in coaxial and on-wafer S-parameters, the development of measurement methods for microwave and terahertz electromagnetic materials characterization, and the development of measurement capabilities of electromagnetic field and specific absorption rate.

Gregory Gäumann received the M.Sc. degree in applied physics from the University of Bern, Bern, Switzerland, in 2014, and the Ph.D. degree from the University of Bern in 2018, with a focus on the fields of terahertz (THz), material, and laser science.

Soon after, he joined the Federal Institute of Metrology (METAS), Bern, to work on a research project related to the topics of THz frequency metrology and photonics.

Markus Zeier received the Dipl.Phys. degree and the Ph.D. degree in experimental nuclear physics from the University of Basel, Basel, Switzerland, in 1993 and 1999, respectively.

He is currently heading the RF and Microwave Laboratory at the Federal Institute of Metrology (METAS), Bern, Switzerland. His research interests are RF and microwave measurement techniques and measurement uncertainty evaluation.

Dr. Zeier has been a Convenor of the EURAMET TCEM SC-RF and MW from 2010 to 2016. He has been holding the chairmanship of the EURAMAT TC-EM since 2019 and the BIPM CCEM GT-RF since 2014.